Supporting Information for

Comparative host interactomes of the SARS-CoV-2 nonstructural protein 3 and human coronavirus homologs

Katherine M. Almasy[1,3,‡], Jonathan P. Davies[2,3,‡], Lars Plate[1,2,3,*]

[1]Department of Chemistry, [2]Department of Biological Sciences, Vanderbilt University, Nashville, TN, USA [3]Vanderbilt Institute for Infection, Immunology, and Inflammation, Vanderbilt University Medical Center, Nashville, TN, USA

‡ contributed equally

*Corresponding author:

Lars Plate
Departments of Chemistry and Biological Sciences
Vanderbilt University
Nashville, TN 37340
Email: lars.plate@vanderbilt.edu
Phone: (615)-343-3405

TABLE OF CONTENT

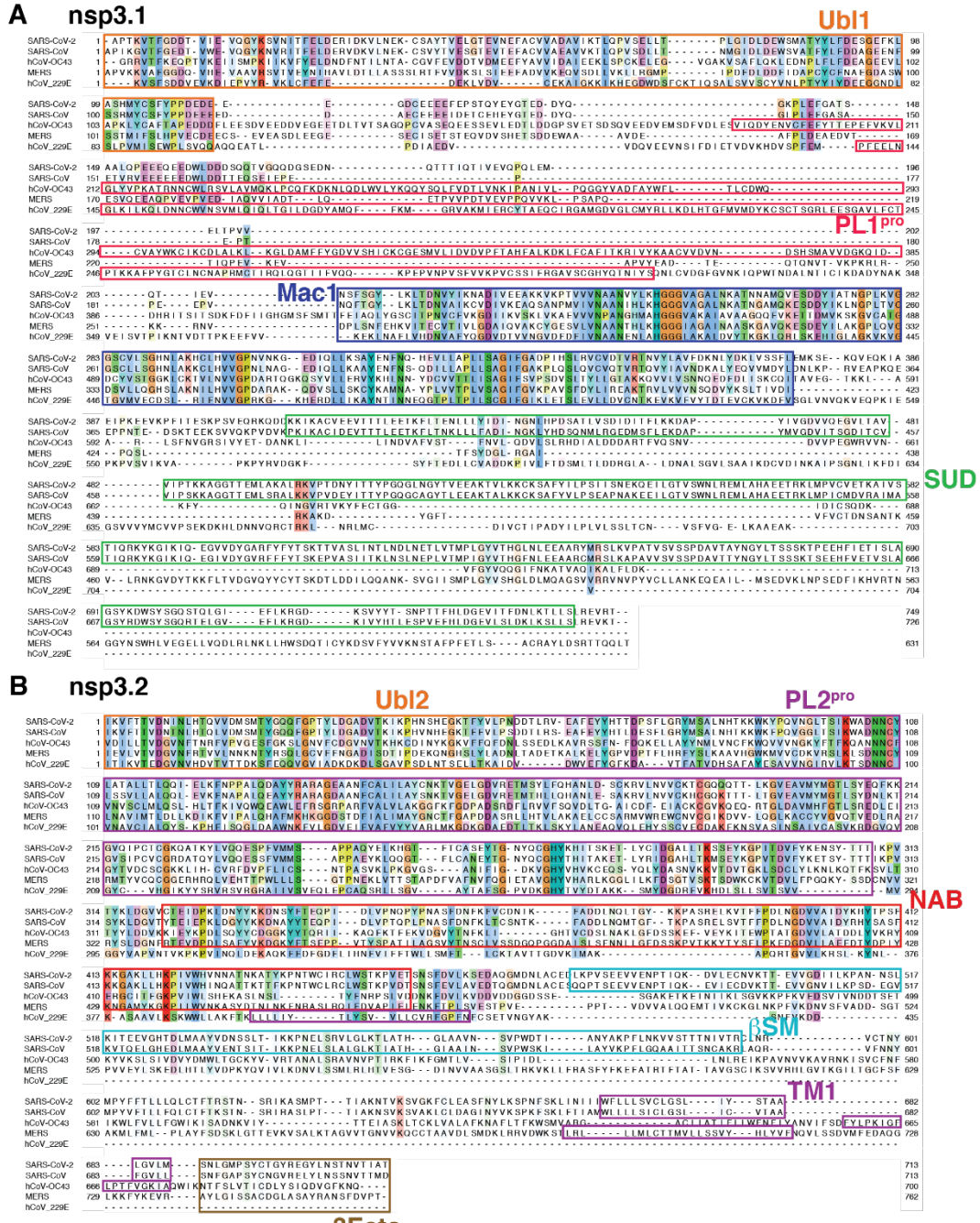
A
nsp3.1
Ubl1
PL1pro
Mac1
SUD
B
nsp3.2
Ubl2
PL2pro
NAB
βSM
TM1
C
nsp3.3
3Ecto_N
3Ecto_C
TM2
AH1
Y & CoV-Y

Figure S1. Multiple-sequence alignment and domain organization of amino acid sequences for nsp3 truncations from different coronavirus strains.

A-C. Amino acid sequences of nsp3.1 (A), nsp3.2 (B), and nsp3.3 (C) homologs were aligned using Clustal Omega. Domain organization is noted by colored boxes[1].

A.

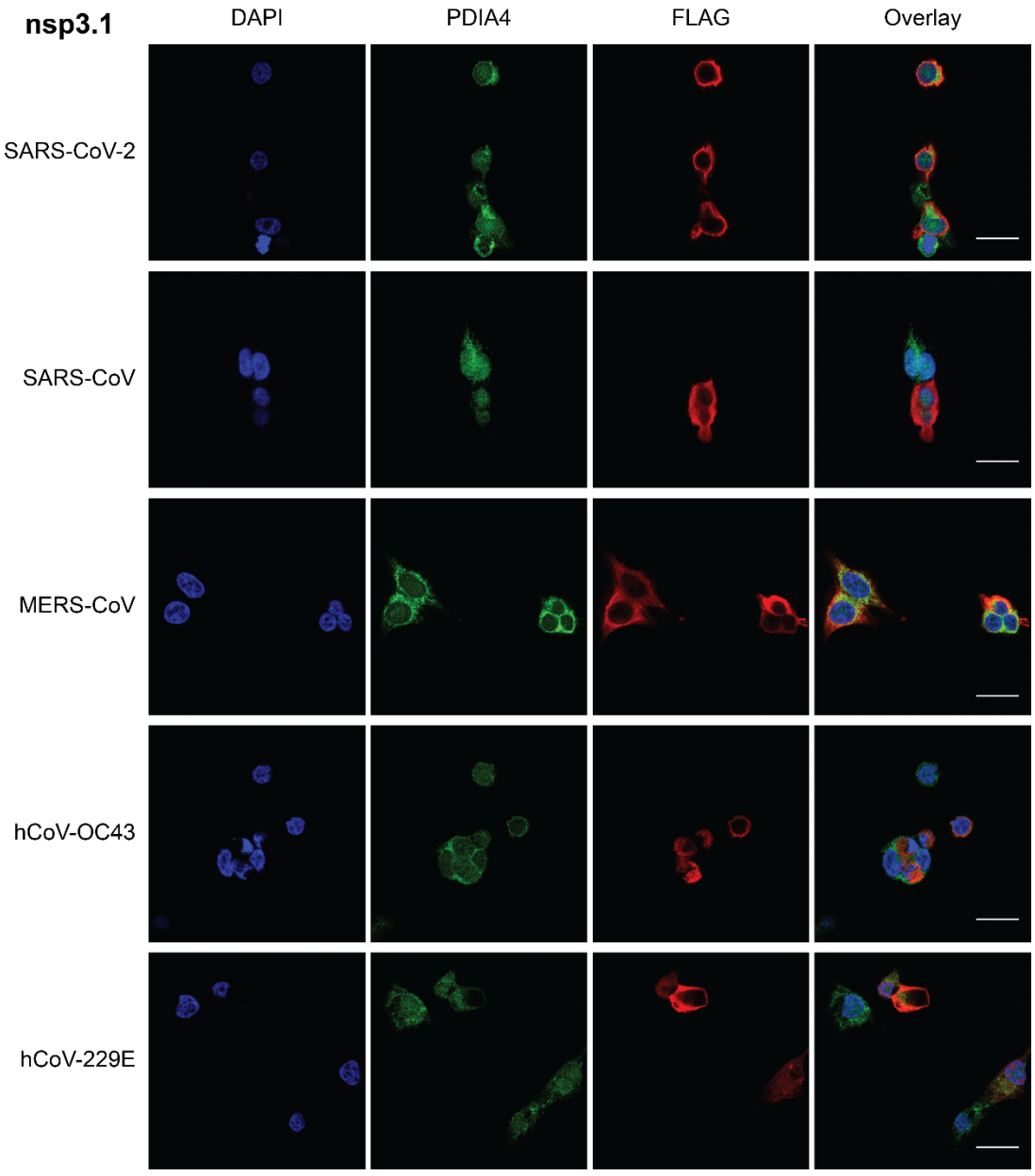

B.

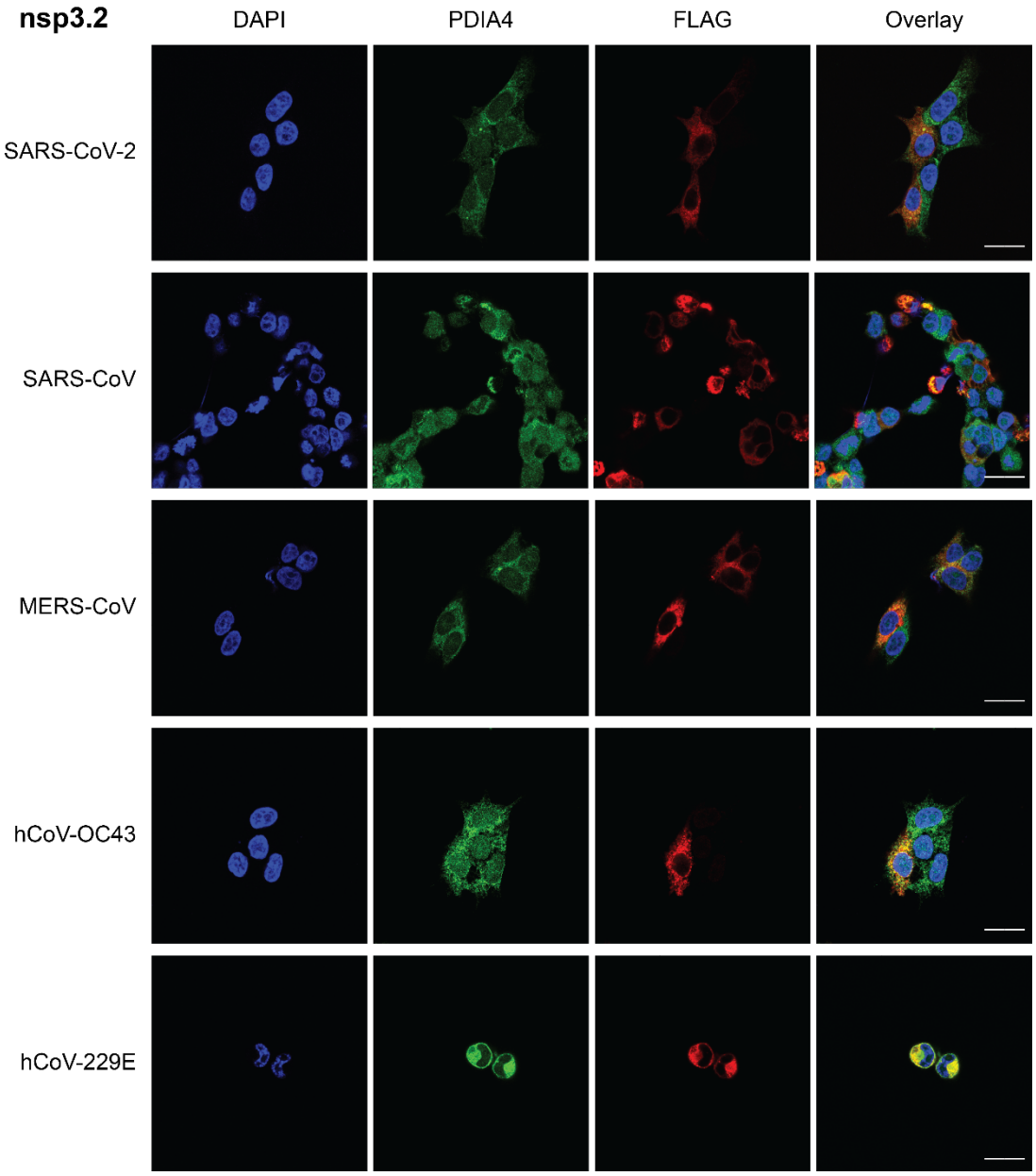
nsp3.2
DAPI
PDIA4
FLAG
Overlay
SARS-CoV-2
SARS-CoV
MERS-CoV
hCoV-OC43
hCoV-229E

C.

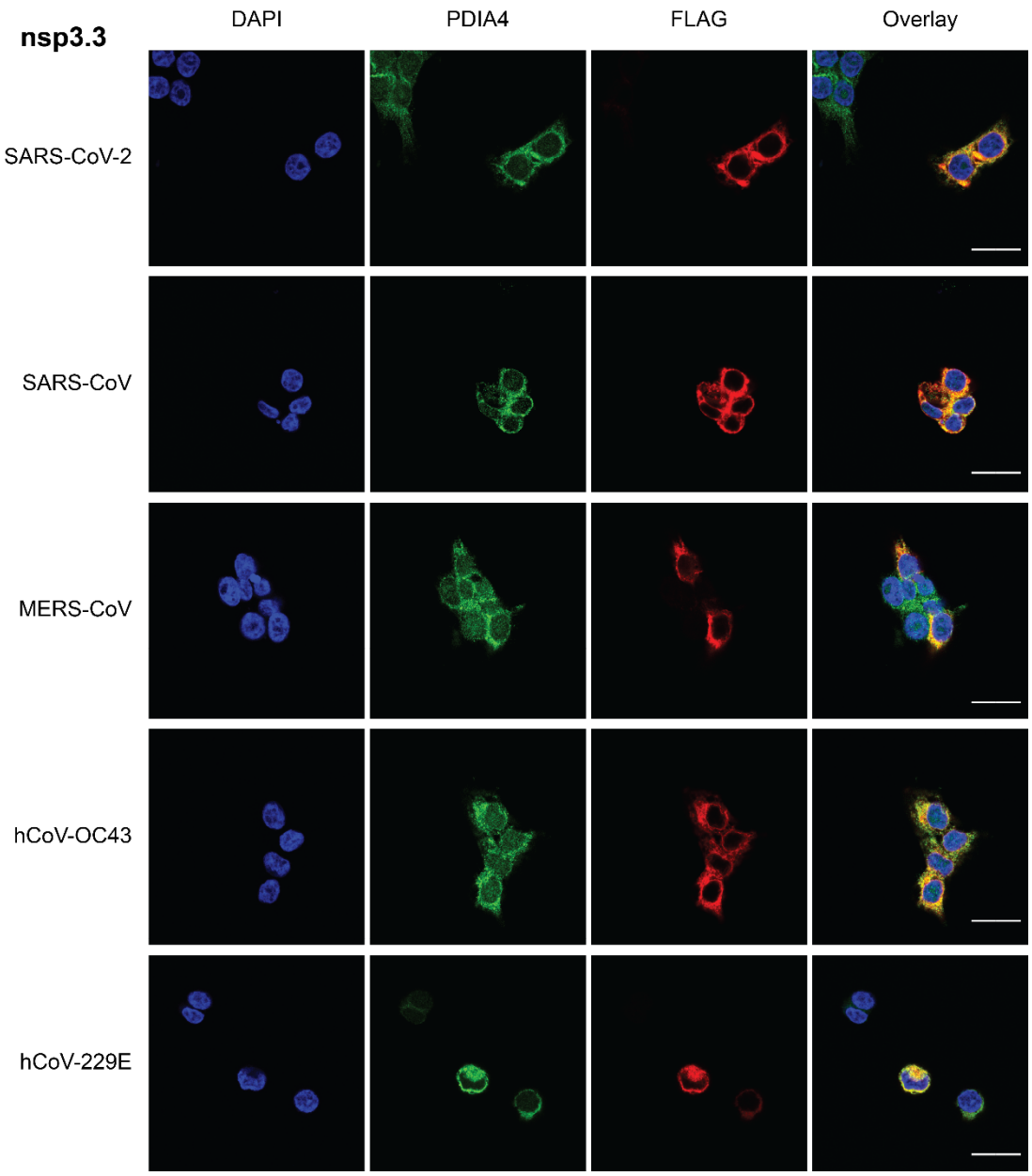

Figure S2. Immunofluorescence confocal imaging of nsp3 fragments.

A.-C. Colocalization of nsp3 fragment FLAG-tagged homologs (red) with the ER marker, PDIA4 (green), in HEK293T cells. Representative images shown. Scale bar is 20 μm. (**A**) nsp3.1 is predominantly localized diffusely cytosolic. (**B**) nsp3.2 and (**C**) nsp3.3 show greater co-localization with the ER maker PDIA4 confirming ER localization.

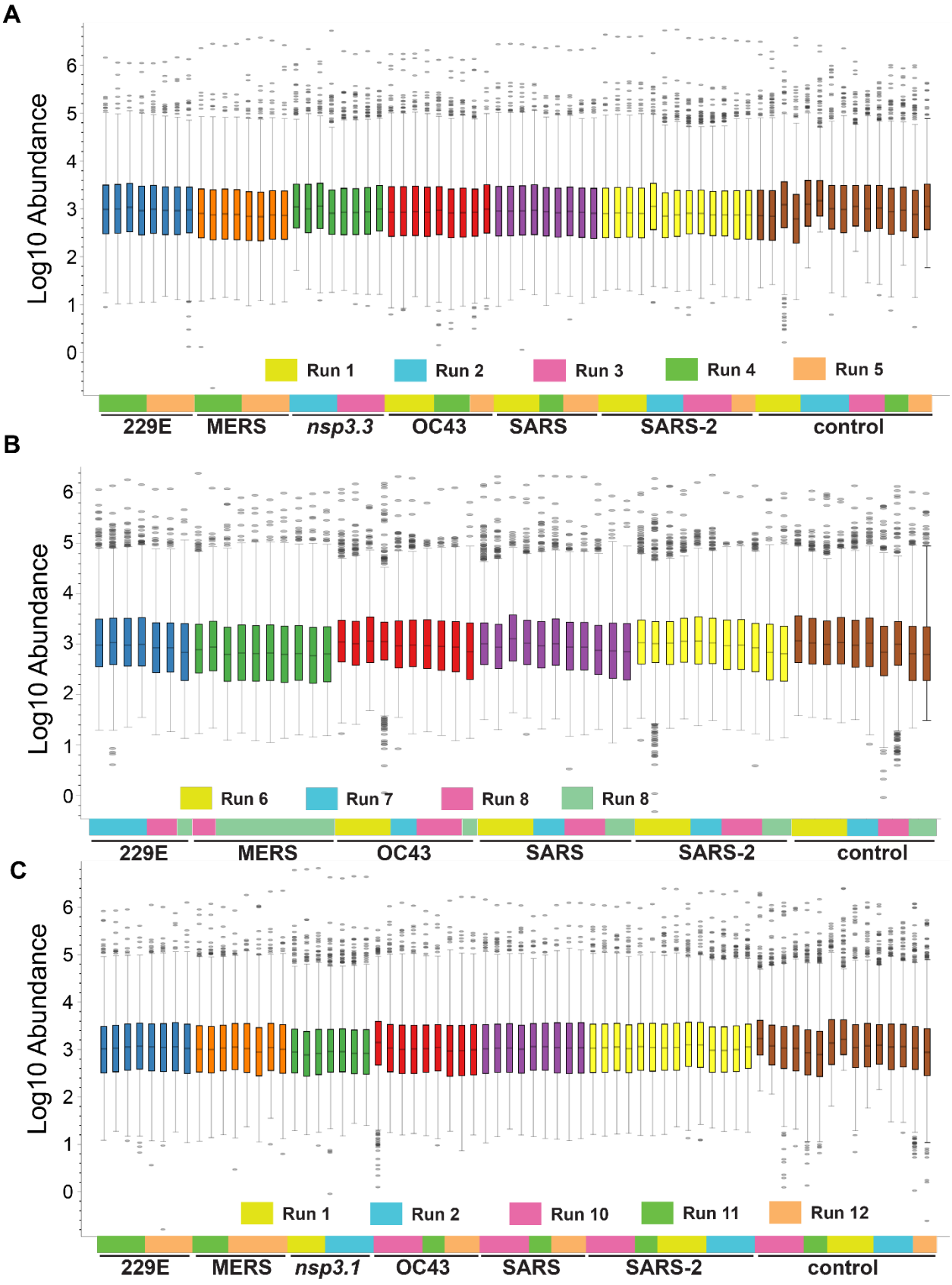
A
Log10 Abundance
0
1
2
3
4
5
6
Run 1
Run 2
Run 3
Run 4
Run 5
229E
MERS
nsp3.3
OC43
SARS
SARS-2
control
B
Log10 Abundance
0
1
2
3
4
5
6
Run 6
Run 7
Run 8
Run 8
229E
MERS
OC43
SARS
SARS-2
control
C
Log10 Abundance
0
1
2
3
4
5
6
Run 1
Run 2
Run 10
Run 11
Run 12
229E
MERS
nsp3.1
OC43
SARS
SARS-2
control

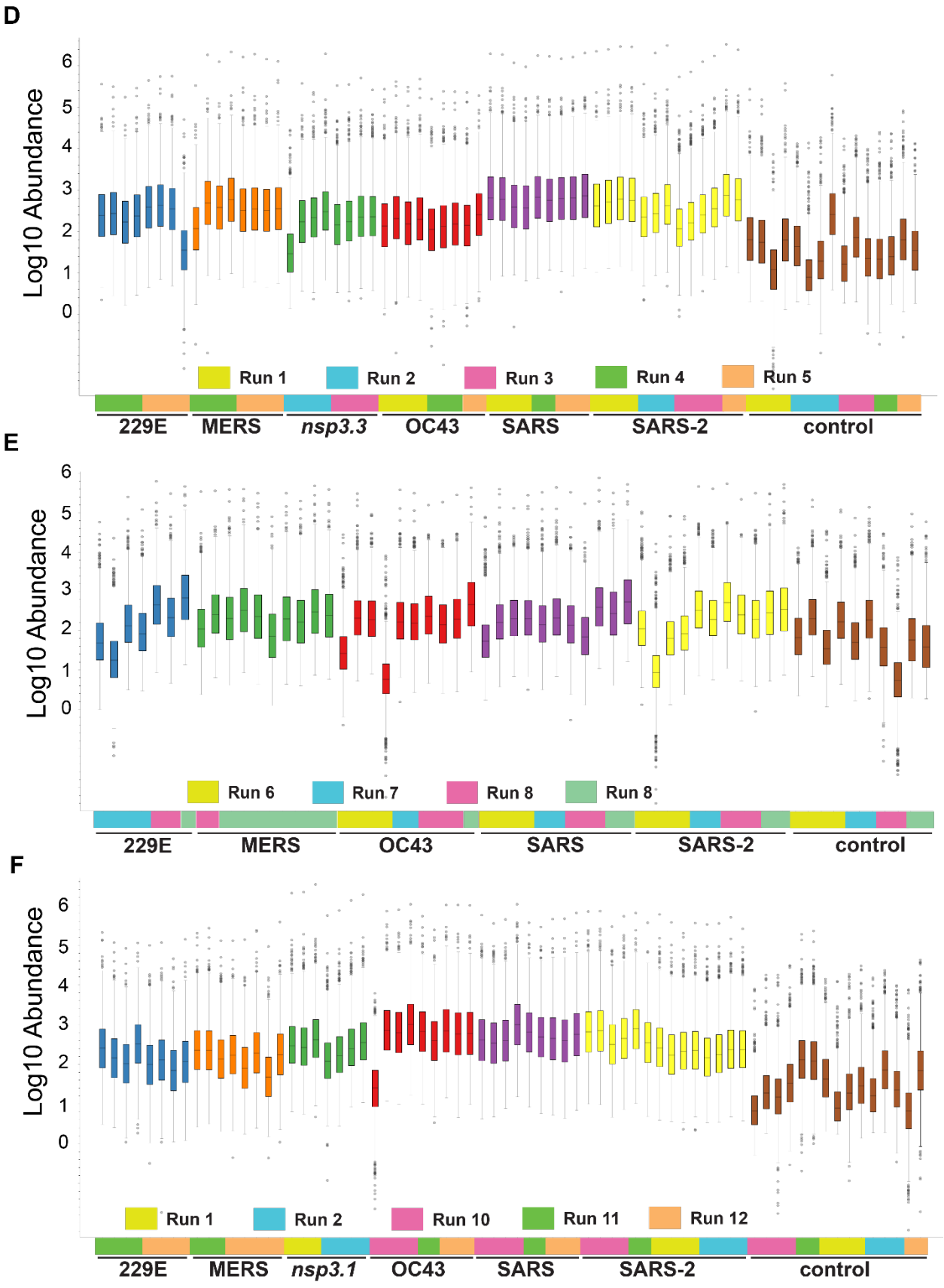
D
Log10 Abundance
0
1
2
3
4
5
6
Run 1
Run 2
Run 3
Run 4
Run 5
229E
MERS
nsp3.3
OC43
SARS
SARS-2
control
E
Log10 Abundance
0
1
2
3
4
5
6
Run 6
Run 7
Run 8
Run 8
229E
MERS
OC43
SARS
SARS-2
control
F
Log10 Abundance
0
1
2
3
4
5
6
Run 1
Run 2
Run 10
Run 11
Run 12
229E
MERS
nsp3.1
OC43
SARS
SARS-2
control

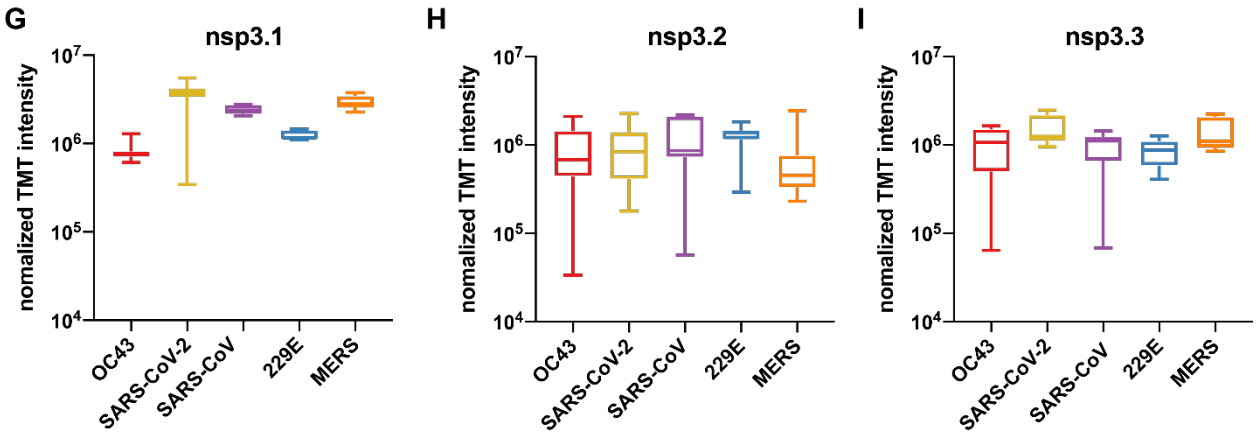

Figure S3. Nsp3 TMT intensity distribution.

A-F. Box-and-whisker plot of the log10 TMT intensity abundance of all 11 mass spectrometry runs used in this study. Nsp3 homologs are grouped by same color box-and-whiskers while the identity of the corresponding mass spectrometry run is denoted by colored blocks below. TMT abundances were normalized based on total peptide amounts (**A-C**). See supporting dataset S8 for the layout of samples across TMT channels.

A,D. Normalized (**A**) and unnormalized (**D**) TMT abundance distribution for nsp3.1 dataset. Channels denoted "*nsp3.3*" were used for the nsp3.3 dataset within the corresponding mass spectrometry run.

B,E. Normalized (**B**) and unnormalized (**E**) TMT abundance distribution for nsp3.2 dataset.

C,F. Normalized (**C**) and unnormalized (**F**) TMT abundance distribution for nsp3.3 dataset. Channels denoted "*nsp3.1*" were used for the nsp3.1 dataset within the corresponding mass spectrometry run.

G-I. Normalized TMT abundances of nsp3 bait proteins to compare the enrichment of fragments from the different strains. Box and whisker blots represent min. to max. values. (**G**) nsp3.1, (**H**) nsp3.2, (**I**) nsp3.3.

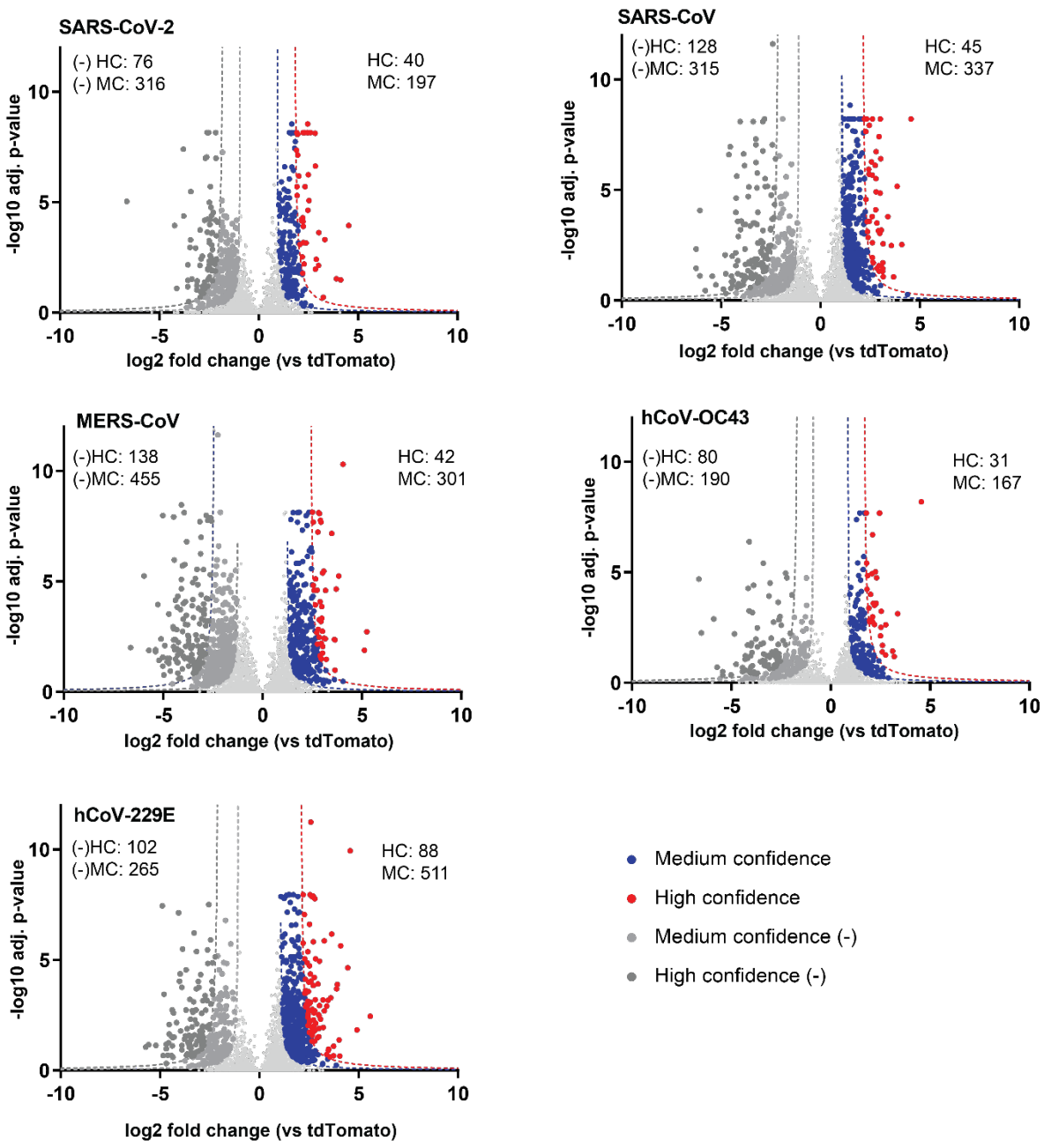

Figure S4. Volcano plots of nsp3.1 homolog high-confidence interactors enriched vs tdTomato control.

Host interactors of nsp3.1 homologs were identified by quantitative proteomics and graphed by log2 fold change compared to tdTomato control and -log10 adjusted *p*-value (based on ANOVA). Interactors were filtered for medium (blue) and high (red) confidence interactors based on a hyperbolic curve using 1σ (medium-confidence) or 2σ (high-confidence) standard deviations of the histogram of log2 protein abundance fold changes (refer to "Data analysis" in Methods). Negative medium- and high-confidence (MC, HC) interactors were calculated in a similar manner. Total MC and HC interactors for positive and negative fold change are indicated respectively.

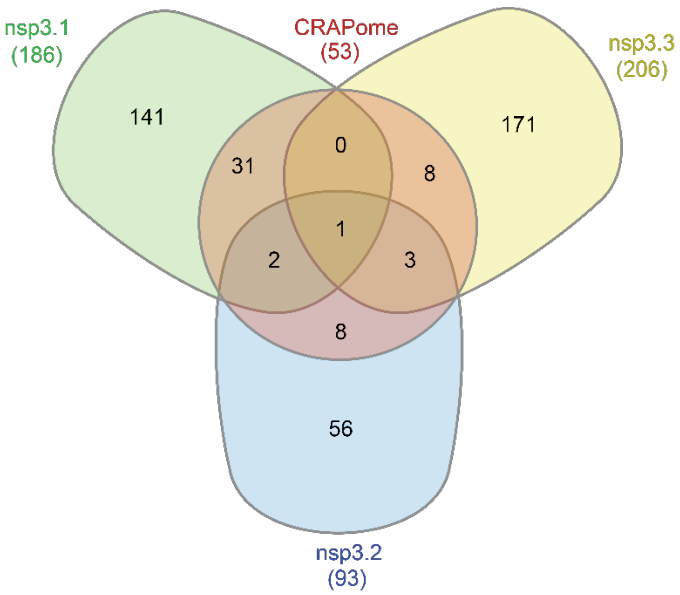

Figure S5. CRAPome overlap with nsp3.1, nsp3.2, and nsp3.3 homolog high-confidence interactors. All high-confidence interactors of nsp3 fragments were queried in the CRAPome *Homo sapiens* single step epitope tag AP-MS dataset to identify common contaminant proteins[2]. Interactors with a frequency of 25% or higher in CRAPome control experiments qualified as overlapping with the CRAPome.

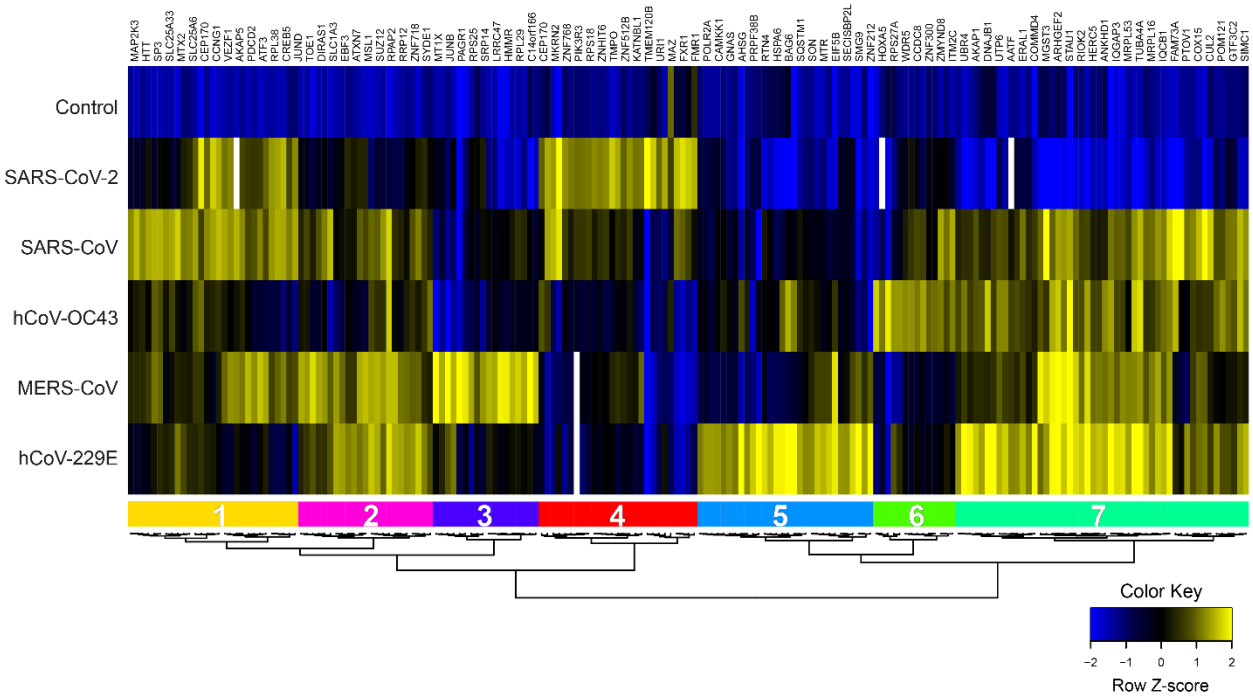

Figure S6. Comparative heatmap of nsp3.1 high-confidence interactors. Unbiased hierarchical clustering of log2 fold change for high-confidence interactors of nsp3.1 homologs yields 7 unique clusters.

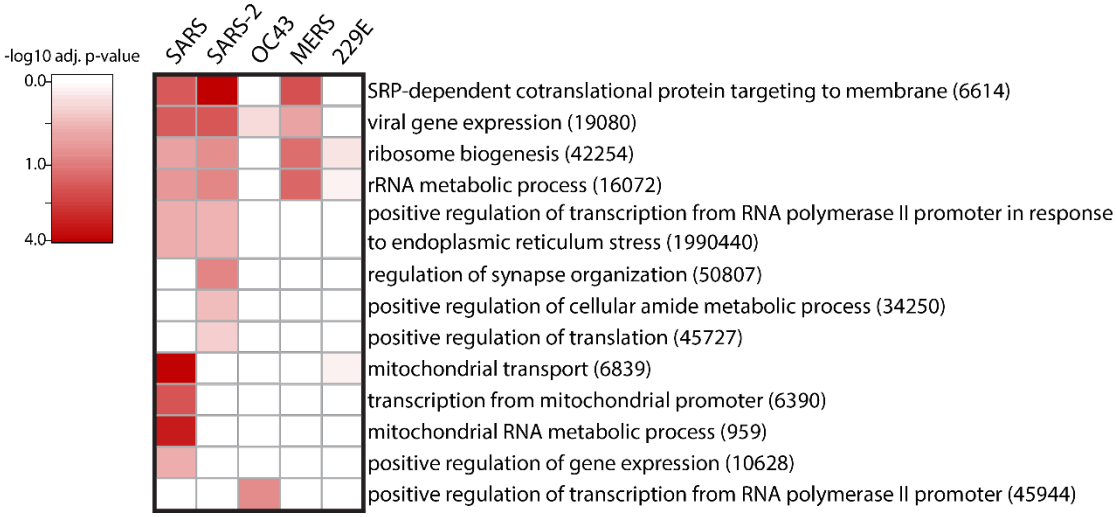

Figure S7. GO term analysis of nsp3.1 high-confidence interactors.
Heatmap of gene ontology (GO) term analysis of nsp3.1 high-confidence interactors for enriched biological processes. Selected terms are displayed with corresponding -log10 adjusted *p*-value for each homolog.

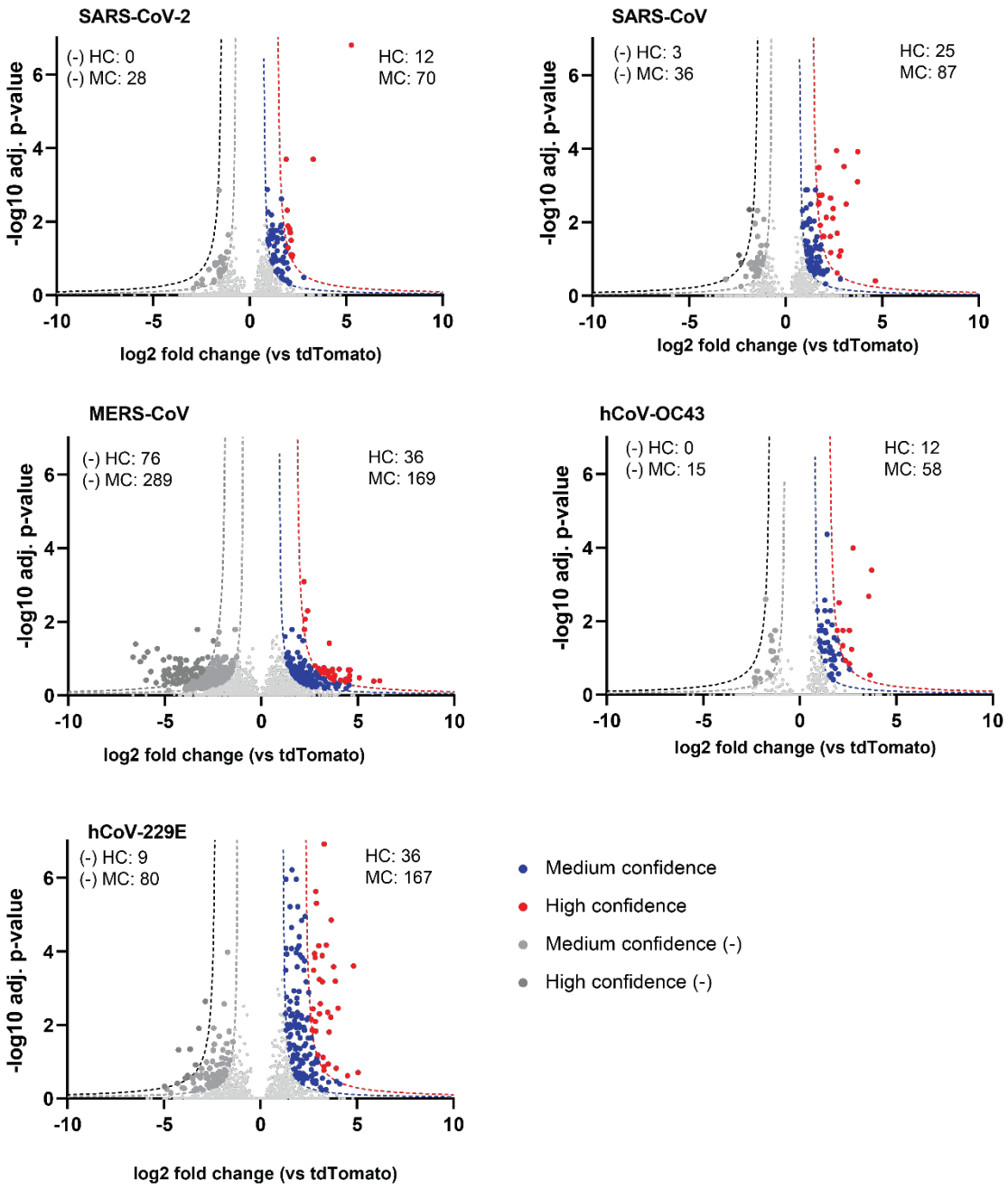

Figure S8. Volcano plots of nsp3.2 homolog high-confidence interactors enriched vs tdTomato control.

Host interactors of nsp3.2 homologs were identified by quantitative proteomics and graphed by log2 fold change compared to tdTomato control and -log10 adjusted *p*-value (based on ANOVA). Interactors were filtered for medium (blue) and high (red) confidence interactors based on a hyperbolic curve using 1σ (medium-confidence) or 2σ (high-confidence) standard deviations of the histogram of log2 protein abundance fold changes (refer to “Data analysis” in Methods). Negative medium- and high-confidence (MC, HC) interactors were calculated in a similar manner. Total MC and HC interactors for positive and negative fold change are indicated respectively.

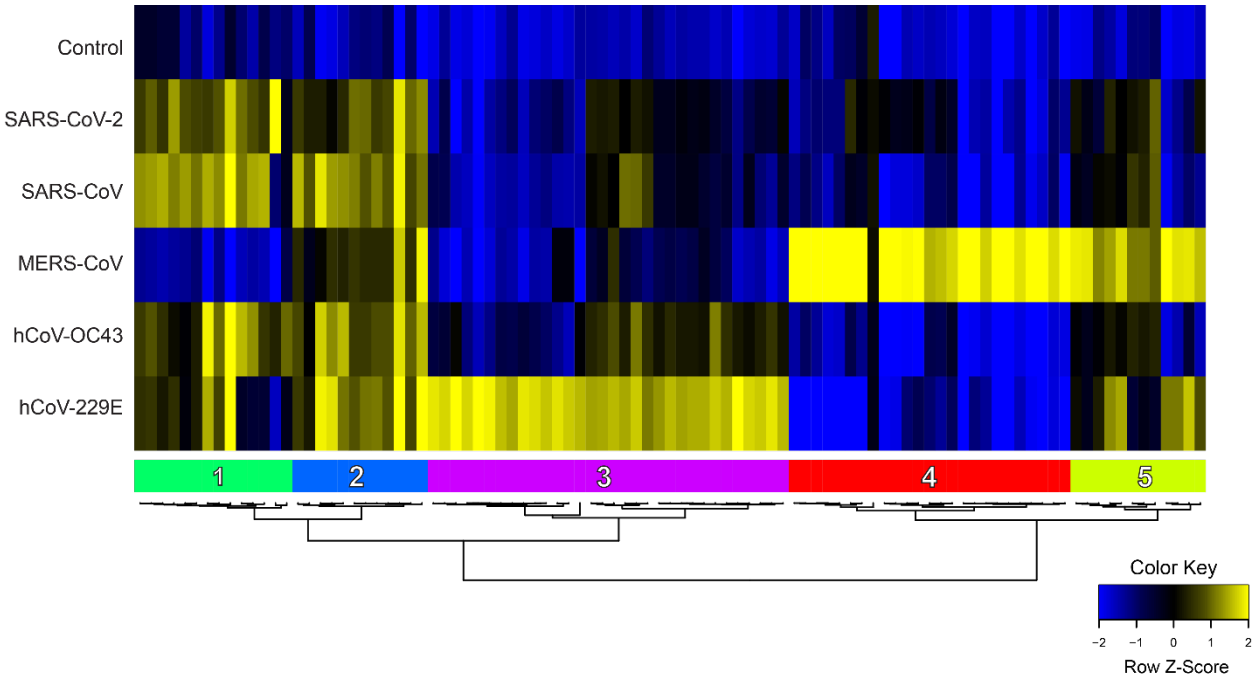

Figure S9. Comparative heatmap of nsp3.2 high-confidence interactors.
Unbiased hierarchical clustering of log2 fold change for high-confidence interactors of nsp3.2 homologs yields 5 unique clusters.

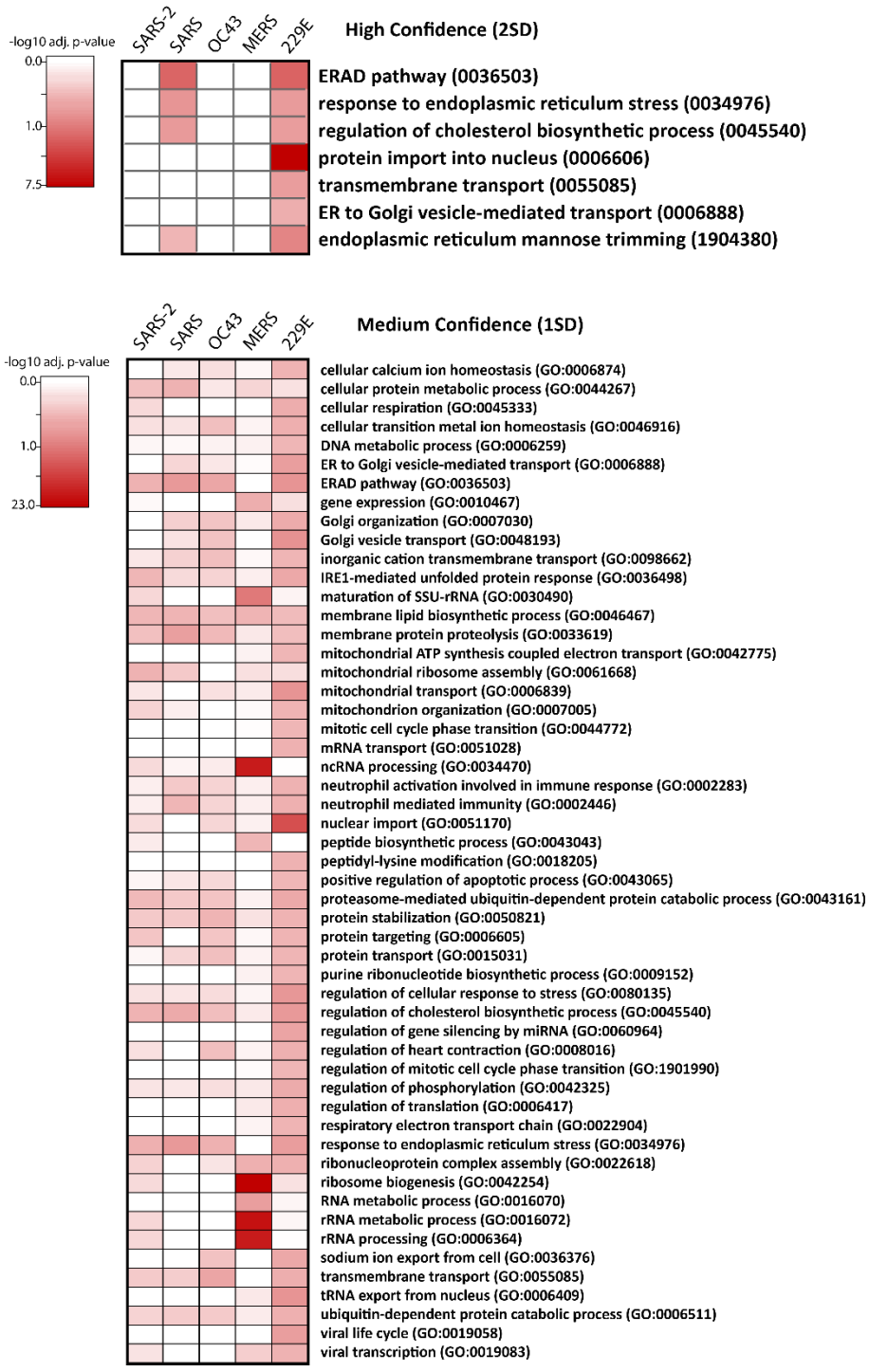

Figure S10. GO term analysis of nsp3.2 high-confidence interactors.
Heatmap of gene ontology (GO) term analysis of nsp3.2 high-confidence or medium-confidence interactors for enriched biological processes. Selected terms are displayed with corresponding -log10 adjusted *p*-value for each homolog.

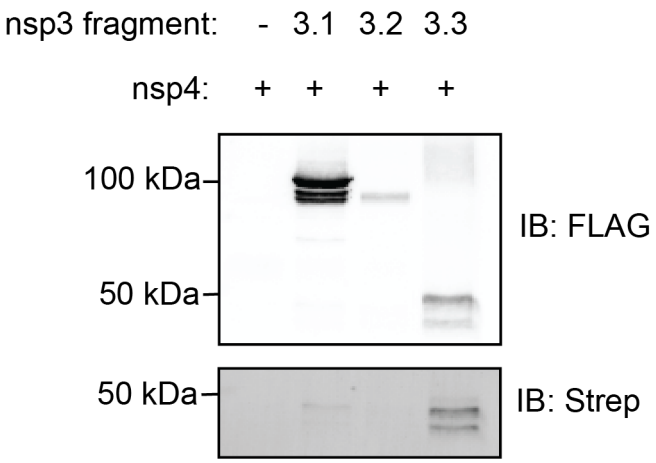

Figure S11. Nsp3 fragment co-immunoprecipitations with nsp4.
Samples were co-transfected with 2x-strep tagged SARS-CoV-2 nsp4[3] and individual SARS-CoV-2 FLAG-tagged nsp3 fragments (nsp3.1, nsp3.2, nsp3.3) or tdTomato as a control, respectively. FLAG immunoprecipitations were performed to pull down on nsp3 constructs and immunoblotting was performed with an anti-FLAG antibody to confirm nsp3.3 expression and an FITC anti-Strep antibody to monitor nsp4 co-immunoprecipitation.

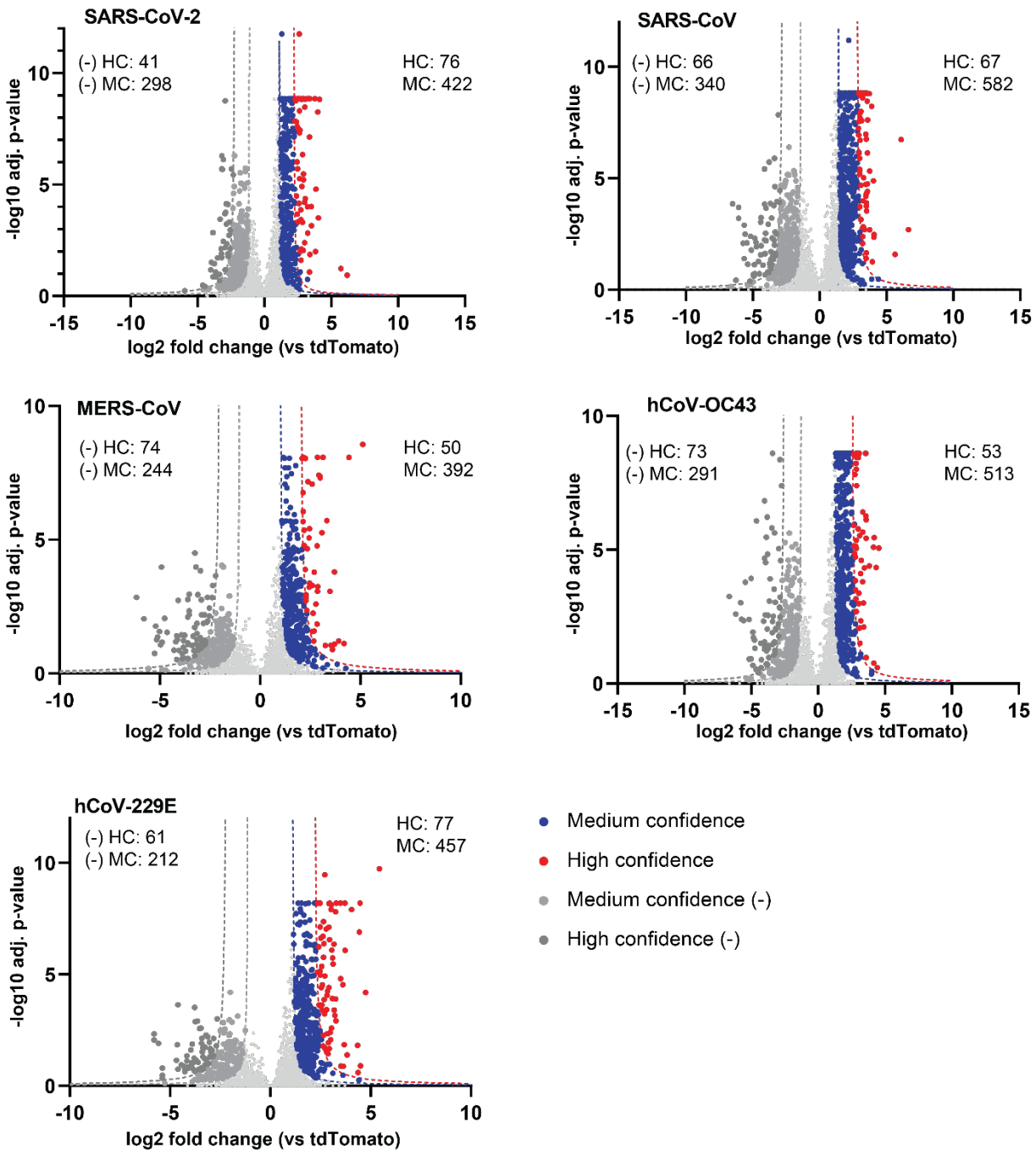

Figure S12. Volcano plots of nsp3.3 homolog high-confidence interactors enriched vs tdTomato control.

Host interactors of nsp3.3 homologs were identified by quantitative proteomics and graphed by log2 fold change compared to tdTomato control and -log10 adjusted *p*-value (based on ANOVA). Interactors were filtered for medium (blue) and high (red) confidence interactors based on a hyperbolic curve using 1σ (medium-confidence) or 2σ (high-confidence) standard deviations of the histogram of log2 protein abundance fold changes (refer to "Data analysis" in Methods). Negative medium- and high-confidence (MC, HC) interactors were calculated in a similar manner. Total MC and HC interactors for positive and negative fold change are indicated respectively.

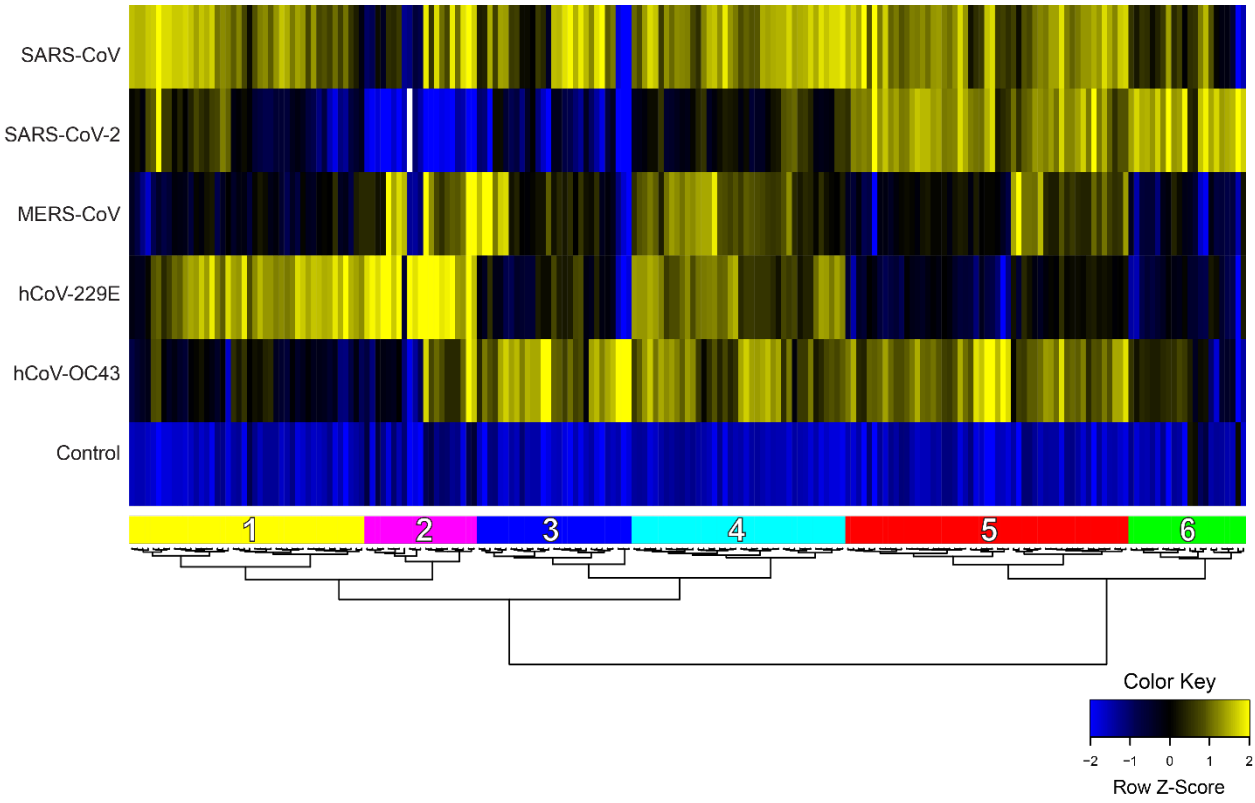

Figure S13. Comparative heatmap of nsp3.3 high-confidence interactors.
Unbiased hierarchical clustering of log2 fold change for high-confidence interactors of nsp3.3 homologs yields 6 unique clusters.

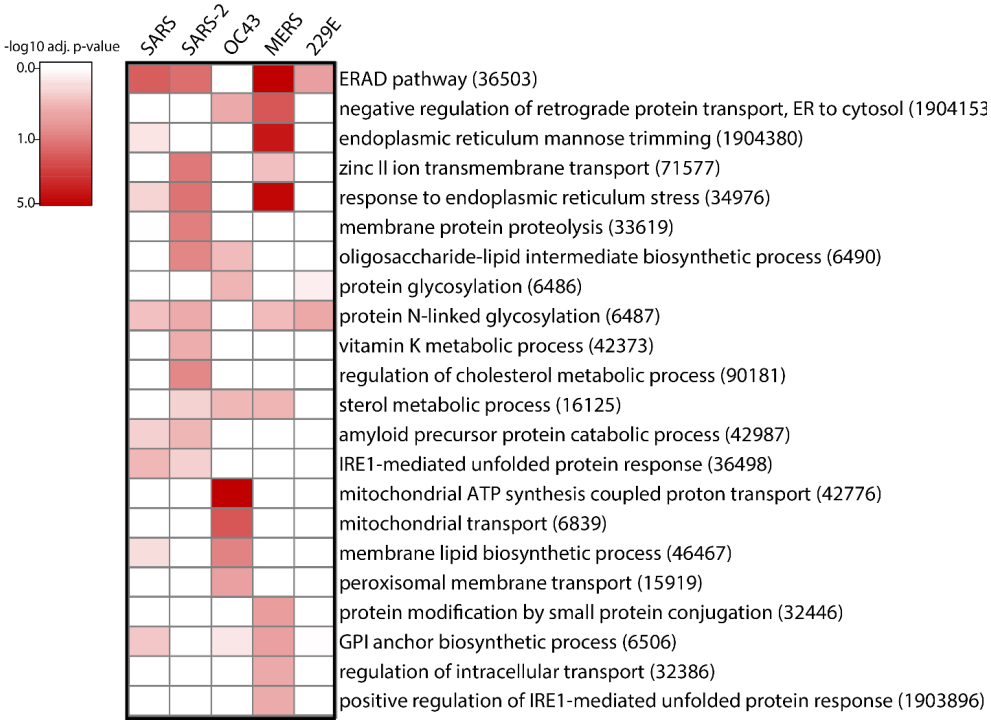

Figure S14. GO term analysis of nsp3.3 high-confidence interactors.
Heatmap of gene ontology (GO) term analysis of nsp3.3 high-confidence or medium-confidence interactors for enriched biological processes. Selected terms are displayed with corresponding -log10 adjusted *p*-value for each homolog.

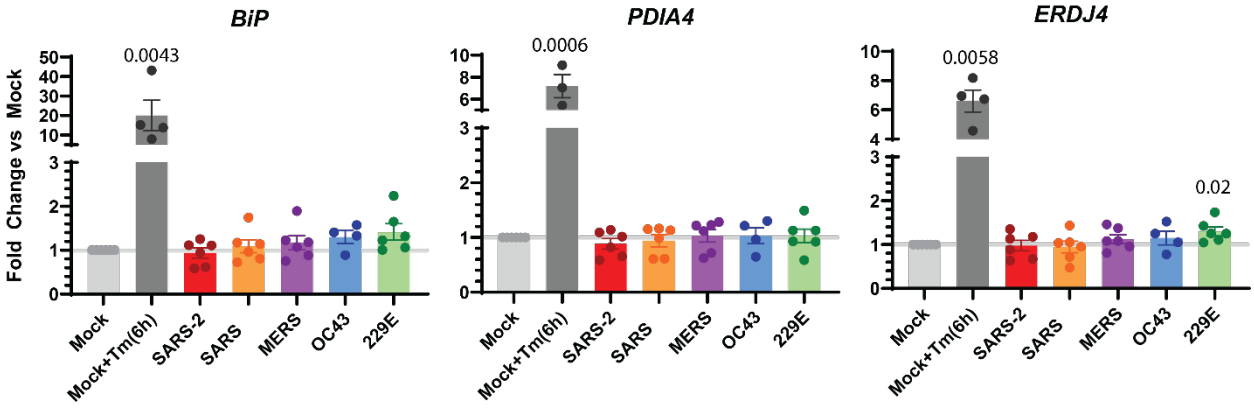

Figure S15. Effect of nsp3.1 homologs on UPR transcript expression.
Expression changes of UPR marker transcripts in response to nsp3.1 homolog or mock (tdTomato) transfection measured by reverse transcription qPCR (RT-qPCR). A mock transfected sample was treated with 6 µg/mL Tunicamycin (Tm) 6 h pre-harvest to induce general UPR activation as a positive control. *BiP* and *PDIA4* were measured as ATF6 markers, while *ERDJ4* was measured as a IRE1/XBP1s marker. Bars indicate average, error bars indicate SEM. Paired student T-tests were used to test for significance, with *p*-values < 0.05 shown. Mock+Tm(6h), n = 4 biological replicates; all other samples, n = 6 biological replicates.

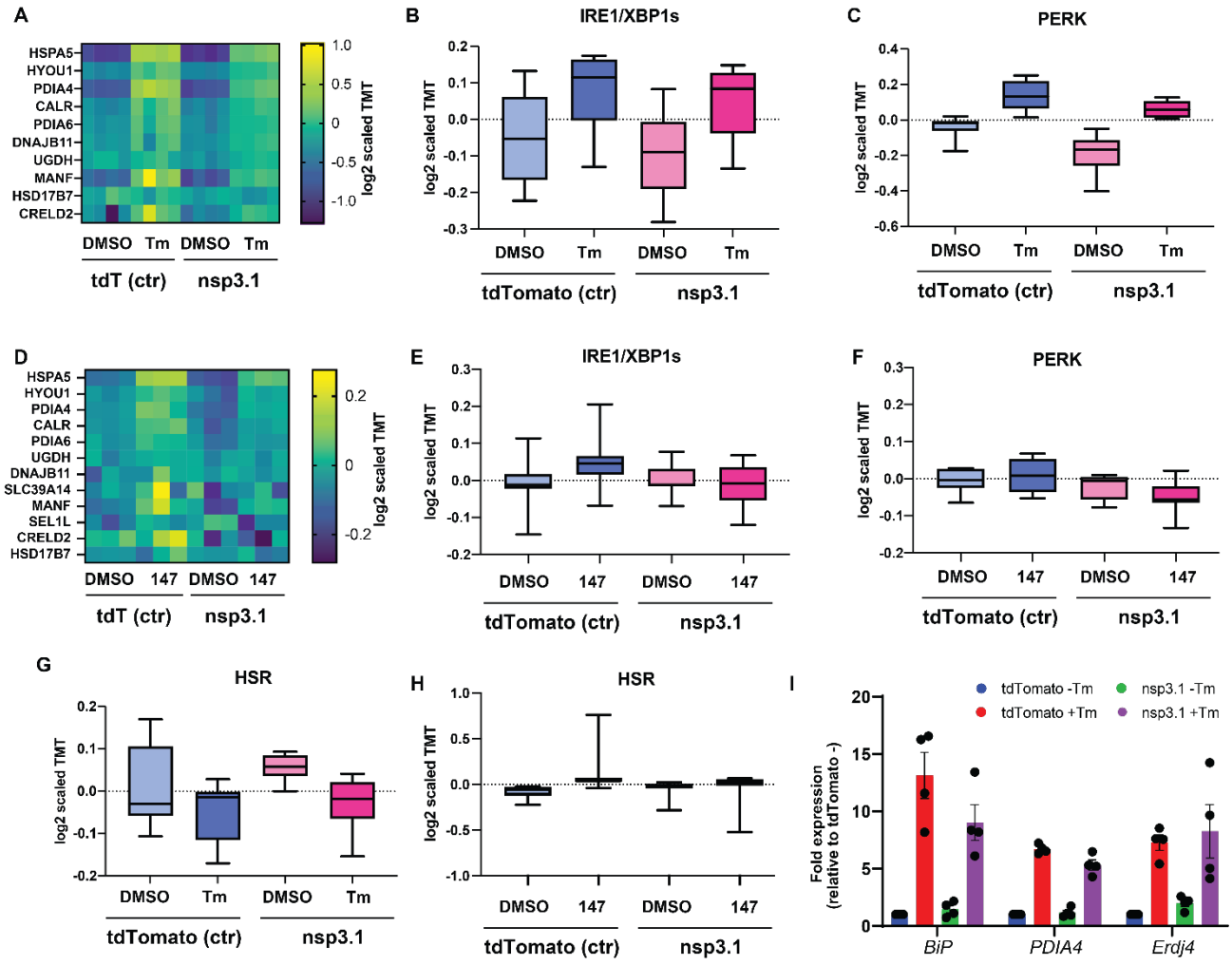

Figure S16. IRE1, PERK UPR, and HSR activation by SARS-CoV-2 nsp3.1

A-C, G. Heatmap of ATF6 UPR signaling branch protein markers (**A**), box-and-whisker plots showing distribution of protein makers of IRE1/XBP1s (**B**) and PERK (**C**) UPR signaling branches and the cytosolic heat shock response (HSR) pathway (**G**) as measured by quantitative proteomics. HEK293T cells were transfected with tdTomato (control) or SARS-CoV-2 nsp3.1-FT. Samples were treated with DMSO or 6 µg/mL tunicamycin for 16 h pre-harvest. A one-way ANOVA with Geisser-Greenhouse correction and post-hoc Tukey's multiple comparison test was used to determine significance (adjusted *p*-values all > 0.05). *n* = 4 biological replicates in a single mass spectrometry run.

D-F, H. Heatmap of ATF6 UPR signaling branch protein markers (**A**) and box-and-whisker plots showing distribution of protein makers of IRE1/XBP1s (**B**) and PERK (**C**) UPR signaling branches and HSR pathway (**H**) as measured by quantitative proteomics. HEK293T cells were transfected with tdTomato (control) or SARS-CoV-2 nsp3.1-FT. Samples were treated with DMSO or 10 µM **147** for 16 h pre-harvest. A one-way ANOVA with Geisser-Greenhouse correction and post-hoc Tukey's multiple comparison test was used to determine significance (adjusted *p*-values all > 0.05). *n* = 3 biological replicates in a single mass spectrometry run.

I. Expression changes of ATF6 (*BiP*, *PDIA4*) and IRE1/XBP1s (*Erdj4*) markers in response to SARS-CoV-2 nsp3.1 or mock (tdTomato) transfection. Where indicated, tunicamycin (Tm) samples were treated 6 hours prior to harvest. Paired ratio t-tests were used to measure significance (n = 4 biological replicates)

SUPPORTING DATASETS

(all supporting tables are available as separate Excel files)

Table S1. Proteomics data of comparative nsp3.1 interactome profiling. Included are protein identifications, quantifications, abundance ratios, statistical analysis, and filtering of medium- and high-confidence interactors.

Table S2. List of peptide identifications, quantifications, and protein mapping for comparative nsp3.1 interactome profiling.

Table S3. Proteomics data of comparative nsp3.2 interactome profiling. Included are protein identifications, quantifications, abundance ratios, statistical analysis, and filtering of medium- and high-confidence interactors.

Table S4. List of peptide identifications, quantifications, and protein mapping for comparative nsp3.2 interactome profiling.

Table S5. Proteomics data of comparative nsp3.3 interactome profiling. Included are protein identifications, quantifications, abundance ratios, statistical analysis, and filtering of medium- and high-confidence interactors.

Table S6. List of peptide identifications, quantifications, and protein mapping for comparative nsp3.3 interactome profiling.

Table S7. Global proteomics data of nsp3.1 modulation of the UPR and associated pathways. Included are protein identifications, quantifications, abundance ratios, statistical analysis, and filtering of UPR and related pathway markers.

Table S8. TMT channel organization for all quantitative proteomics experiments.

SUPPORTING INFORMATION REFERENCES

(1) Lei, J.; Kusov, Y.; Hilgenfeld, R. Nsp3 of Coronaviruses: Structures and Functions of a Large Multi-Domain Protein. *Antiviral Research*. Elsevier B.V. January 1, 2018, pp 58–74. https://doi.org/10.1016/j.antiviral.2017.11.001.

(2) Mellacheruvu, D.; Wright, Z.; Couzens, A. L.; Lambert, J. P.; St-Denis, N. A.; Li, T.; Miteva, Y. V.; Hauri, S.; Sardiu, M. E.; Low, T. Y.; Halim, V. A.; Bagshaw, R. D.; Hubner, N. C.; Al-Hakim, A.; Bouchard, A.; Faubert, D.; Fermin, D.; Dunham, W. H.; Goudreault, M.; Lin, Z. Y.; Badillo, B. G.; Pawson, T.; Durocher, D.; Coulombe, B.; Aebersold, R.; Superti-Furga, G.; Colinge, J.; Heck, A. J. R.; Choi, H.; Gstaiger, M.; Mohammed, S.; Cristea, I. M.; Bennett, K. L.; Washburn, M. P.; Raught, B.; Ewing, R. M.; Gingras, A. C.; Nesvizhskii, A. I. The CRAPome: A Contaminant Repository for Affinity Purification-Mass Spectrometry Data. *Nat. Methods* **2013**, *10* (8), 730–736. https://doi.org/10.1038/nmeth.2557.

(3) Gordon, D. E.; Jang, G. M.; Bouhaddou, M.; Xu, J.; Obernier, K.; White, K. M.; O'Meara, M. J.; Rezelj, V. V.; Guo, J. Z.; Swaney, D. L.; Tummino, T. A.; Hüttenhain, R.; Kaake, R. M.; Richards, A. L.; Tutuncuoglu, B.; Foussard, H.; Batra, J.; Haas, K.; Modak, M.; Kim, M.; Haas, P.; Polacco, B. J.; Braberg, H.; Fabius, J. M.; Eckhardt, M.; Soucheray, M.; Bennett, M. J.; Cakir, M.; McGregor, M. J.; Li, Q.; Meyer, B.; Roesch, F.; Vallet, T.; Mac Kain, A.; Miorin, L.; Moreno, E.; Naing, Z. Z. C.; Zhou, Y.; Peng, S.; Shi, Y.; Zhang, Z.; Shen, W.; Kirby, I. T.; Melnyk, J. E.; Chorba, J. S.; Lou, K.; Dai, S. A.; Barrio-Hernandez, I.; Memon, D.; Hernandez-Armenta, C.; Lyu, J.; Mathy, C. J. P.; Perica, T.; Pilla, K. B.; Ganesan, S. J.; Saltzberg, D. J.; Rakesh, R.; Liu, X.; Rosenthal, S. B.; Calviello, L.; Venkataramanan, S.; Liboy-Lugo, J.; Lin, Y.; Huang, X. P.; Liu, Y. F.; Wankowicz, S. A.; Bohn, M.; Safari, M.; Ugur, F. S.; Koh, C.; Savar, N. S.; Tran, Q. D.; Shengjuler, D.; Fletcher, S. J.; O'Neal, M. C.; Cai, Y.; Chang, J. C. J.; Broadhurst, D. J.; Klippsten, S.;

Sharp, P. P.; Wenzell, N. A.; Kuzuoglu-Ozturk, D.; Wang, H. Y.; Trenker, R.; Young, J. M.; Cavero, D. A.; Hiatt, J.; Roth, T. L.; Rathore, U.; Subramanian, A.; Noack, J.; Hubert, M.; Stroud, R. M.; Frankel, A. D.; Rosenberg, O. S.; Verba, K. A.; Agard, D. A.; Ott, M.; Emerman, M.; Jura, N.; von Zastrow, M.; Verdin, E.; Ashworth, A.; Schwartz, O.; d'Enfert, C.; Mukherjee, S.; Jacobson, M.; Malik, H. S.; Fujimori, D. G.; Ideker, T.; Craik, C. S.; Floor, S. N.; Fraser, J. S.; Gross, J. D.; Sali, A.; Roth, B. L.; Ruggero, D.; Taunton, J.; Kortemme, T.; Beltrao, P.; Vignuzzi, M.; García-Sastre, A.; Shokat, K. M.; Shoichet, B. K.; Krogan, N. J. A SARS-CoV-2 Protein Interaction Map Reveals Targets for Drug Repurposing. *Nature* **2020**, *583* (7816), 459–468. https://doi.org/10.1038/s41586-020-2286-9.